AIP | Physics of Fluids

Onset of double-diffusive convection in a rectangular cavity with stress-free upper boundary

Zhi-Wu Chen, Jie-Min Zhan, Yok-Sheung Li, and Yu-Hua Nie

Citation: Phys. Fluids **22**, 124101 (2010); doi: 10.1063/1.3517296
View online: http://dx.doi.org/10.1063/1.3517296
View Table of Contents: http://pof.aip.org/resource/1/PHFLE6/v22/i12
Published by the American Institute of Physics.

Onset of double-diffusive convection in a rectangular cavity with stress-free upper boundary

Zhi-Wu Chen,[1] Jie-Min Zhan,[1,a)] Yok-Sheung Li,[2] and Yu-Hua Nie[3]
[1]*Department of Applied Mechanics and Engineering, Sun Yat-sen University, Guangzhou 510275, China*
[2]*Department of Civil and Structural Engineering, The Hong Kong Polytechnic University, Hong Kong, China*
[3]*South China Sea Branch, State Oceanic Administration, Guangzhou 510300, China*

(Received 14 June 2010; accepted 21 October 2010; published online 1 December 2010)

Double-diffusive buoyancy convection in an open-top rectangular cavity with horizontal temperature and concentration gradients is considered. Attention is restricted to the case where the opposing thermal and solutal buoyancy effects are of equal magnitude (buoyancy ratio $R_\rho=-1$). In this case, a quiescent equilibrium solution exists and can remain stable up to a critical thermal Grashof number Gr_c. Linear stability analysis and direct numerical simulation show that depending on the cavity aspect ratio A, the first primary instability can be oscillatory, while that in a closed cavity is always steady. Near a codimension-two point, the two leading real eigenvalues merge into a complex coalescence that later produces a supercritical Hopf bifurcation. As Gr further increases, this complex coalescence splits into two real eigenvalues again. The oscillatory flow consists of counter-rotating vortices traveling from right to left and there exists a critical aspect ratio below which the onset of convection is always oscillatory. Neutral stability curves showing the influences of A, Lewis number Le, and Prandtl number Pr are obtained. While the number of vortices increases as A decreases, the flow structure of the eigenfunction does not change qualitatively when Le or Pr is varied. The supercritical oscillatory flow later undergoes a period-doubling bifurcation and the new oscillatory flow soon becomes unstable at larger Gr. Random initial fields are used to start simulations and many different subcritical steady states are found. These steady states correspond to much stronger flows when compared to the oscillatory regime. The influence of Le on the onset of steady flows and the corresponding heat and mass transfer properties are also investigated.
 [doi:10.1063/1.3517296]

I. INTRODUCTION

The density of a fluid can be influenced simultaneously by heat and solute with different diffusivities. In a gravitational field, this can generate many intriguing flow phenomena, even when the overall density distribution is stable. Due to its great importance in geology and many industrial processes, this double-diffusive buoyancy convection has been the topic of intensive research for many years.[1–3]

Depending on the applications, different configurations of the temperature and solute concentration gradients have been considered in existing literatures: vertical ∇T and ∇C, horizontal ∇T and ∇C, or vertical ∇C and horizontal ∇T. Here we only mention one special case where these gradients are both horizontal and the resultant thermal and solutal buoyancy forces are opposing and of equal magnitude (buoyancy ratio $R_\rho=-1$). In this case, a quiescent equilibrium corresponding to the pure conductive and diffusive state exists and can remain stable up to a critical thermal Rayleigh number. Krishnan[4] was the first to numerically study in a square cavity the transition from the equilibrium regime to the steady convective regime. Further transitions to periodic and quasiperiodic flows with up to three incommensurate frequencies were also obtained. Gobin and Bennacer[5] studied the onset of convection in an infinite vertical layer with impermeable and slip boundary conditions. The situation in a finite cavity with no-slip boundary condition was also considered and a turning point of the subcritical solution branch was confused with the critical bifurcation point of the quiescent equilibrium. Later, Ghorayeb and Mojtabi[6] studied this problem more systematically. They showed that the primary instability of the equilibrium corresponds to a transcritical bifurcation point that is determined by $\mathrm{Ra}_c(\mathrm{Le}-1)$, where Ra_c is the critical Rayleigh number and Le is the Lewis number. The onset of oscillatory flow as a function of Le was studied by Ghorayeb *et al.*[7] Nonlinear bifurcation analysis[8,9] has been done and extensions of the configuration to an inclined cavity[10] and to porous cavities[11,12] have also been considered. More recently, the situation in a three-dimensional enclosure was studied by Bergeon and Knobloch.[13] These two authors also investigated the multiplicity of stable spatially localized steady states, a phenomenon known as "homoclinic snaking" that can be interpreted in terms of a pinning region in the parameter space.[14] The onset of subcritical convection was predicted by Ouriemi *et al.*[15]

Like buoyancy force, liquid surface tension can also be simultaneously influenced by temperature and solute concentration. A similar configuration to the above mentioned special case is when the upper rigid wall of the cavity is removed and the thermal and solutal Marangoni effects due to

a)Author to whom correspondence should be addressed. Electronic mail: cejmzhan@gmail.com.

horizontal temperature and concentration gradients are equal and opposing (solutal to thermal Marangoni number ratio $R_\sigma=-1$). Then a purely diffusive quiescent equilibrium also exists and can remain stable up to a certain critical thermal Marangoni number, beyond which convection occurs. Bergman[16] was the first to study this so-called double-diffusive Marangoni instability in the absence of buoyancy. Some steady flow states were obtained using direct numerical simulation. However, the nature of the primary bifurcation point had long remained unclear. Very recently, this problem was studied systematically by Chen *et al.*,[17] where it was shown by both linear stability analysis and direct simulation that the first primary instability of the equilibrium corresponds to a supercritical Hopf bifurcation. The flow arising from small disturbance is oscillatory rather than steady. Transition to chaos has also been considered by Li *et al.*[18]

Double-diffusive buoyancy convection in an open-top cavity was studied by Younis *et al.*,[19] where Marangoni effects were neglected and the results were compared to those in a closed cavity to evaluate the influence of the upper rigid boundary. However, the onset of convection in this configuration when the buoyancy ratio $R_\rho=-1$ has never been explored. It has been found that in a closed cavity, the two most unstable modes are all steady (transcritical and pitchfork), and their neutral stability curves cross successively at a series of codimension-two bifurcation points as the aspect ratio increases.[8,10] No new dynamical behavior is produced near these codimension-two points and the onset of convection is always steady. We find that, however, when the upper rigid wall is removed and the upper boundary becomes stress-free, the first primary instability of the equilibrium can be a Hopf bifurcation, i.e., the flow arising from small disturbance can be oscillatory, rather than always steady. It is the purpose of the present paper to investigate the onset of convection in such an open-top cavity when the thermal and solutal buoyancy effects due to horizontal temperature and concentration gradients are equal and opposing ($R_\rho=-1$).

The rest of this paper is organized as follows. In Sec. II, the definition of the physical problem and the mathematical formulation are given. Solution methods including linear stability analysis and direct numerical simulation are described in Sec. III. Results and discussions are presented in Sec. IV, where it is shown that the transcritical and pitchfork steady modes can mix together to produce an oscillatory mode near codimension-two points, and in certain parameter range many different subcritical steady states coexist. Finally, the conclusions are included in Sec. V.

II. PROBLEM DEFINITION

The two-dimensional rectangular cavity is made up of three rigid walls, of length L and height H, and filled with a binary fluid with a nondeformable liquid-air surface on the top (Fig. 1). Different temperatures and concentrations are specified at the left (T_1, C_1) and right (T_2, C_2) vertical walls, where $T_1 > T_2$ and $C_1 > C_2$, and zero heat and mass fluxes are imposed on the two horizontal boundaries. The no-slip boundary condition is adopted for all velocity components on the rigid walls, and on the upper surface Marangoni effect

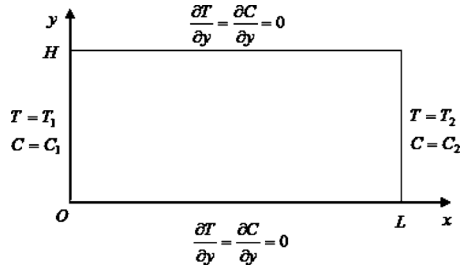

FIG. 1. Schematic of the physical system.

is neglected. Boussinesq approximation is assumed to be valid except for the density ρ, which is allowed to vary linearly with liquid temperature and solute concentration. Thus,

$$\rho(T,C)=\rho_0[1-\beta_T(T-T_0)-\beta_C(C-C_0)], \tag{1}$$

where $\rho_0=\rho(T_0,C_0)$, $\beta_T=(-1/\rho_0)(\partial\rho/\partial T)_C$, and $\beta_C=(-1/\rho_0)(\partial\rho/\partial C)_T$. The thermophysical properties of the fluid are estimated at the reference temperature T_0 and concentration C_0, which are set to be equal to T_2 and C_2, respectively.

By choosing L as the unit of length and υ/L as the unit of velocity, where υ denotes the kinematic viscosity of the fluid, the nondimensionalized equations governing the conservation of mass, momenta, energy, and solute concentration can be written as

$$\nabla\cdot V=0, \tag{2}$$

$$\frac{\partial V}{\partial t}+(V\cdot\nabla)V=-\nabla p+\nabla^2 V+\mathrm{Gr}(\theta+R_\rho\cdot c)\vec{j}, \tag{3}$$

$$\frac{\partial\theta}{\partial t}+(V\cdot\nabla)\theta=\frac{1}{\mathrm{Pr}}\nabla^2\theta, \tag{4}$$

$$\frac{\partial c}{\partial t}+(V\cdot\nabla)c=\frac{1}{\mathrm{Pr}\cdot\mathrm{Le}}\nabla^2 c, \tag{5}$$

together with boundary conditions

$$x=0,\quad y\in[0,A]:u=v=0,\quad \theta=c=1, \tag{6}$$

$$x=1,\quad y\in[0,A]:u=v=0,\quad \theta=c=0, \tag{7}$$

$$y=0,\quad x\in[0,1]:u=v=0,\quad \frac{\partial\theta}{\partial y}=\frac{\partial c}{\partial y}=0, \tag{8}$$

$$y=A,\quad x\in[0,1]:\frac{\partial u}{\partial y}=0,\quad v=0,\quad \frac{\partial\theta}{\partial y}=\frac{\partial c}{\partial y}=0, \tag{9}$$

where $V=u\cdot\vec{i}+v\cdot\vec{j}$ is the velocity vector. There are five dimensionless parameters in the above system,

$$A=\frac{H}{L},\quad \mathrm{Pr}=\frac{\upsilon}{\alpha},\quad \mathrm{Le}=\frac{\alpha}{D},\quad \mathrm{Gr}=\frac{g\beta_T\Delta TL^3}{\upsilon^2},\quad R_\rho=\frac{\beta_C\Delta C}{\beta_T\Delta T}, \tag{10}$$

which are respectively the aspect ratio, the Prandtl number, the Lewis number, the thermal Grashof number, and the

buoyancy ratio. α denotes thermal diffusivity and D the molecular diffusivity. Gr is related to the classic Rayleigh number by $\mathrm{Ra}=\mathrm{Gr}\cdot\mathrm{Pr}$. In the present study, attention is restricted to the special case $R_\rho=-1$, in which the thermal and solutal buoyancy forces exactly balance each other and the no-flow equilibrium solution can remain stable up to a critical thermal Grashof number.

The average heat and mass fluxes at the left vertical wall are given by the Nusselt and Sherwood numbers as

$$\mathrm{Nu}=\frac{1}{A}\int_0^A\left|\frac{\partial\theta}{\partial x}\right|_{x=0}dy \tag{11}$$

and

$$\mathrm{Sh}=\frac{1}{A}\int_0^A\left|\frac{\partial c}{\partial x}\right|_{x=0}dy. \tag{12}$$

III. SOLUTION METHODS

A. Linear stability analysis

The linear stability characteristics of the equilibrium solutions $u_0=v_0=0$, $\theta_0=1-x$, and $c_0=1-x$ obtained for $R_\rho=-1$ are studied. In a standard way, infinitesimal disturbances are applied to the systems (2)–(9), and after linearization the following system is obtained:

$$\begin{cases}\nabla\cdot V=0\\ \dfrac{\partial V}{\partial t}=-\nabla p+\nabla^2V+\mathrm{Gr}(\theta-c)\vec{j}\\ \dfrac{\partial\theta}{\partial t}-u=\dfrac{1}{\mathrm{Pr}}\nabla^2\theta\\ \dfrac{\partial c}{\partial t}-u=\dfrac{1}{\mathrm{Pr}\cdot\mathrm{Le}}\nabla^2c,\end{cases} \tag{13}$$

together with boundary conditions

$$\begin{cases}x=0,\ \ y\in[0,A]:u=v=0,\ \ \theta=c=0\\ x=1,\ \ y\in[0,A]:u=v=0,\ \ \theta=c=0\\ y=0,\ \ x\in[0,1]:u=v=0,\ \ \dfrac{\partial\theta}{\partial y}=\dfrac{\partial c}{\partial y}=0\\ y=A,\ \ x\in[0,1]:\dfrac{\partial u}{\partial y}=0,\ \ v=0,\ \ \dfrac{\partial\theta}{\partial y}=\dfrac{\partial c}{\partial y}=0.\end{cases} \tag{14}$$

The dependent variables $V=u\cdot\vec{i}+v\cdot\vec{j}, p, \theta$ and c now denote small disturbances. In order to eliminate the pressure terms, the stream function $\psi(\partial\psi/\partial y=u,\ -\partial\psi/\partial x=v)$ is introduced and the system becomes

$$\begin{cases}\dfrac{\partial}{\partial t}\Delta\psi=\Delta^2\psi-\mathrm{Gr}\left(\dfrac{\partial\theta}{\partial x}-\dfrac{\partial c}{\partial x}\right)\\ \dfrac{\partial\theta}{\partial t}=\dfrac{\partial\psi}{\partial y}+\dfrac{1}{\mathrm{Pr}}\Delta\theta\\ \dfrac{\partial c}{\partial t}=\dfrac{\partial\psi}{\partial y}+\dfrac{1}{\mathrm{Le}\cdot\mathrm{Pr}}\Delta c,\end{cases} \tag{15}$$

with boundary conditions

$$\begin{cases}x=0,\ \ 1,\ \ y\in[0,A]:\psi=\dfrac{\partial\psi}{\partial x}=0,\ \ \theta=c=0\\ y=0,\ \ x\in[0,1]:\psi=\dfrac{\partial\psi}{\partial y}=0,\ \ \dfrac{\partial\theta}{\partial y}=\dfrac{\partial c}{\partial y}=0\\ y=A,\ \ x\in[0,1]:\psi=\dfrac{\partial^2\psi}{\partial y^2}=0,\ \ \dfrac{\partial\theta}{\partial y}=\dfrac{\partial c}{\partial y}=0.\end{cases} \tag{16}$$

The eigenvalue problem defined by Eqs. (15) and (16) is solved by the Tau spectral method.[20] The time dependence of disturbances is assumed to be of exponential form with a complex growth factor $\lambda=\sigma+i\omega$, while the spatial distributions are represented by series of Chebyshev polynomials. Thus, the variables are written as

$$\psi(t,x,y)=e^{\lambda t}\sum_{n=0}^{N}\sum_{m=0}^{M}a_{nm}T_n(x)T_m(y), \tag{17}$$

$$\theta(t,x,y)=e^{\lambda t}\sum_{n=0}^{N}\sum_{m=0}^{M}b_{nm}T_n(x)T_m(y), \tag{18}$$

$$c(t,x,y)=e^{\lambda t}\sum_{n=0}^{N}\sum_{m=0}^{M}c_{nm}T_n(x)T_m(y), \tag{19}$$

where $T_k(x), k=0,1,2,\ldots$ are Chebyshev polynomials of the first kind. Depending on the dimensionless parameters, N and M vary in the range of 14–74 in order for the series to converge. By substituting Eqs. (17)–(19) into Eqs. (15) and (16), a generalized eigenvalue problem with a matrix size of $[3(N+1)(M+1),\ 3(N+1)(M+1)]$ is obtained. The complex eigenvalue λ can be determined when the parameters Gr, Le, Pr, and A are specified. Then one of the parameters, say Gr, is increased until the real part of λ vanishes. The corresponding value of Gr is the critical condition for neutral stability and the imaginary part of λ indicates whether the instability evolves into steady convection or growing oscillation. When the onset is oscillatory, the critical dimensionless oscillation frequency can be determined by $f_c=\omega/2\pi$ and the full oscillation cycle of the flow field can be determined by $\psi(t,x,y)=\xi(x,y)\cdot\cos\omega t-\zeta(x,y)\cdot\sin\omega t$, where $\xi(x,y)$ and $\zeta(x,y)$ are the real and imaginary parts of the corresponding complex eigenfunction, respectively.

B. Direct numerical simulation

Equations (2)–(5) together with the boundary conditions (6)–(9) are discretized using nonuniform control volumes. Finer grids cluster near the boundaries in order to improve the numerical accuracy. Colocated variable arrangement is used and the SIMPLE algorithm is adopted to couple momentum and continuity equations. In searching for steady-state flow, initially very large time step is used for fast convergence. For cases where convergent steady solutions cannot be obtained, small time steps are used to detect possible unsteady behavior. The time stepping is realized by the second order, implicit, three time level scheme. Details of the implementation of the numerical procedures can be found in Ferziger and Peric.[21]

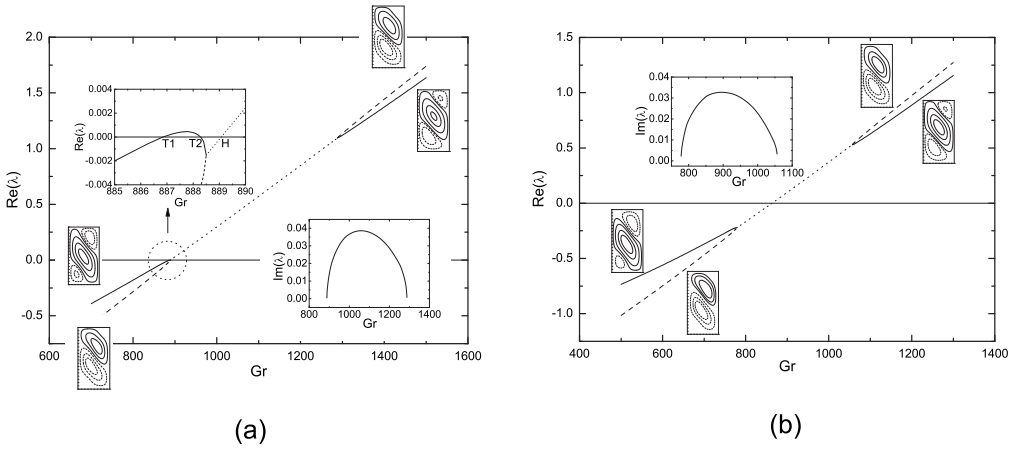

FIG. 2. Variations of real parts of the leading eigenvalues with Gr for Pr=1 and Le=11: (a) $A=1.9$; (b) $A=2$. Solid and dashed lines denote two different steady modes, with the flow structures of the eigenfunctions shown, while the dotted line denotes oscillatory mode. Variations of the imaginary parts of the eigenvalues for the oscillatory modes are also shown as insets.

Validations of both the linear stability analysis and direct numerical simulation procedures were detailed in Chen *et al.*,[17] where these two methods were successfully used to investigate the onset of double-diffusive Marangoni convection in a similar configuration.

IV. RESULTS AND DISCUSSIONS

A. Linear stability analysis

1. Variations of leading eigenvalues with Gr

As the dynamic parameter Gr increases, the eigenvalues in the complex plane move and it is the crossing of the right-most eigenvalues with the imaginary axis that determines the onset of convection. Steady or oscillatory modes may be induced, depending on whether the crossing eigenvalues are real or complex. Thus, it is interesting to see how the leading eigenvalues vary with Gr.

We first investigate the situation for Pr=1 and Le=11. This choice of parameters is motivated by earlier results.[6,10] Variations of the leading eigenvalues when $A=1.9$ are shown in Fig. 2(a). Before the onset of convection $[\mathrm{Re}(\lambda)<0]$, the most unstable mode is a steady mode with the flow field consisting of three vortices, while the second most unstable mode is a steady mode with two vortices (solid and dashed lines denote different rotating directions). In a closed cavity,[8,10] the geometry and the linearized equations are invariant under combined reflection by x and y (or, equivalently, under rotation by π) and by the inversion of the temperature and concentration perturbation fields. Let S denote this centrosymmetry and $X(\psi,\theta,c)$ a steady solution. The operation $S:X\rightarrow S(X)$ is $(\psi,\theta,c)(x,y)\rightarrow(\psi,-\theta,-c)(1-x,A-y)$. Eigenmodes will be either centrosymmetric, i.e., $S(\psi,\theta,c)=(\psi,\theta,c)$, or anticentrosymmetric, i.e., $S(\psi,\theta,c)=-(\psi,\theta,c)$. Centrosymmetric eigenmodes contain an odd number of cells while anticentrosymmetric eigenmodes contain an even number of cells. These two different types of modes are generated by transcritical and pitchfork bifurcations, respectively. In Fig. 2(a), the eigenmodes containing three and two vortices correspond, respectively, to the centrosymmetric and anticentrosymmetric eigenmodes in a closed cavity. However, in the present configuration where the upper boundary is stress-free, this centrosymmetry or anticentrosymmetry can no longer be preserved, e.g., the two small vortices in the upper-right and lower-left corners of the transcritical mode are no longer of the same size. As Gr increases, the growth rates of these two steady modes increase and, as shown by the inset, the transcritical mode first gets onset at the T1 bifurcation point. Then, surprisingly, its growth rate decreases quickly, producing a subcritical steady bifurcation at T2. Finally, it coalesces with the pitchfork mode (dashed line) and an oscillatory mode (dotted line) is produced, i.e., the two real eigenvalues merge into a pair of complex conjugate eigenvalues. As Gr further increases, this oscillatory mode creates a Hopf bifurcation at H. The imaginary part of the complex eigenvalues corresponding to this oscillatory mode is shown as the inset. It can be seen that the dimensionless oscillation frequency increases from zero at the coalescence point, reaches the maximum, and then decreases to zero as Gr increases. When Im(λ) decreases to zero, the pair of complex conjugate eigenvalues splits into two real eigenvalues, which correspond to the transcritical and pitchfork modes before coalescence. This whole coalescence and splitting process is similar to the situation of a 2×2 matrix problem studied by Tuckerman[22] and the Marangoni convection in binary mixtures studied by Bergeon *et al.*[23] It is interesting to note that before coalescence the most unstable mode is transcritical, while after splitting the most unstable mode is pitchfork. In the case of a closed cavity, these two steady modes simply cross at a codimension-two point and near this point no new dynamical behavior is observed.[8,10] However, in our present configuration, due to the broken centrosymmetry of the system, these two steady modes merge into a complex coalescence when they are about to cross, thus producing totally new dynamics: oscillation. That the broken symmetry can play a significant role in determining the system dynamics has also been studied by Ecke *et al.*[24] and Goldstein *et al.*[25,26] for convection in a rotating cylinder. In this prototype problem, these authors

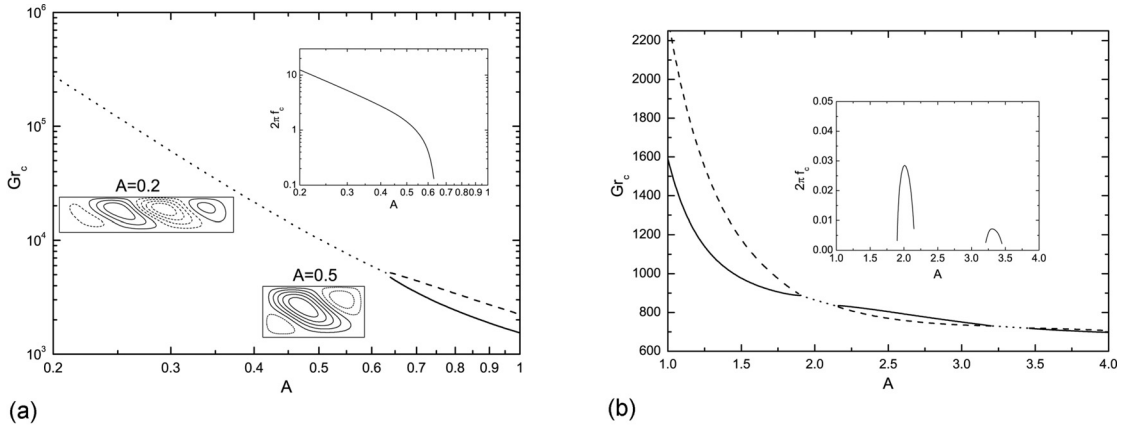

FIG. 3. Neutral stability curves when (a) $A \leq 1$ and (b) $A \geq 1$ for Pr=1 and Le=11. Solid lines denote transcritical modes, dashed lines denote pitchfork modes, and dotted lines denote oscillatory modes. The dimensionless frequencies of the oscillatory modes are also shown as insets.

showed that the broken reflection symmetry turns the steady-state bifurcation in the nonrotating system into a Hopf bifurcation in the rotating system.

The situation when A slightly increases to 2 is shown in Fig. 2(b). The two steady modes coalesce well before Re(λ) becomes positive. The complete neutral stability curves showing the influence of A on the onset of convection will be shown in Sec. IV A 2. Also, the influences of Le and Pr on the onset of oscillatory flow will be considered.

2. Influences of A, Le, and Pr

The neutral stability curves showing the influence of A on the onset of convection are shown in Fig. 3. In the range of aspect ratio studied, the transcritical and pitchfork modes cross successively at a series of codimension-two bifurcation points: $A=0.63$, $A=1.89$, $A=2.16$, $A=3.21$, and $A=3.46$. When $0.63<A<1.89$ and $3.46<A<4$, the first onset of convection is the transcritical mode, while when $2.16<A<3.21$ the first onset of convection is the pitchfork mode. In the other parts of the range of A, the two steady modes merge into an oscillatory mode. The variations of the corresponding oscillation frequency are shown by the insets. The frequency decreases to zero at codimension-two bifurcation points, or equivalently, the period diverges. This is a trademark of the disappearance of the Hopf bifurcation at these points. It is also interesting to note that when A decreases from 0.63, the frequency of the oscillatory mode increases exponentially and there is no sign of decreasing to another codimension-two point. Thus, $A=0.63$ is also a critical aspect ratio below which the onset of convection is always oscillatory.

Steady flows in a vertical closed cavity ($A>1$) have been studied in detail by Bergeon *et al.*,[10] and here we are more focused on the oscillatory flow in a horizontal cavity ($A<1$). The flow structures of the eigenfunctions at the onset of instability when $A=0.2$ and $A=0.5$ are shown as insets in Fig. 3(a). As A decreases, the number of vortices increases. The full oscillation cycle when $A=0.5$ is shown in Fig. 4. It can be seen that counter-rotating vortices travel from right to left. Figure 4(a) corresponds to the steady flow field of the transcritical mode in a closed cavity, while Fig. 4(c) corresponds to that of the pitchfork mode. Thus, it can be understood that the flow field oscillates between the transcritical and the pitchfork modes, or that the oscillatory mode is a mixed mode of the two steady modes. This oscillatory flow field has also been verified by direct numerical simulation.

That the oscillation frequency increases when A decreases from 0.63 *might be* explained as follows: the no-slip boundary condition imposed on the left and right vertical walls will oppose the flow reversal that occurs during each oscillation. As the aspect ratio decreases, the influence of the left and right vertical walls decreases, and thus the oscillation frequency increases. However, this explanation cannot explain why the frequency variation in the other two intervals $1.89<A<2.16$ and $3.21<A<3.46$ is not monotonic, but has a parabolic shape. From Fig. 3(a), it can be seen that in addition to the oscillation frequency, Gr_c also increases exponentially with decreasing A. This means that as A approaches 0, the equilibrium solution becomes linearly infinitely stable. Such infinite stability is of course unphysical. Fully nonlinear direct simulations show that finite amplitude disturbance can set in well before the linear threshold and render the equilibrium state unstable. Since supercritical os-

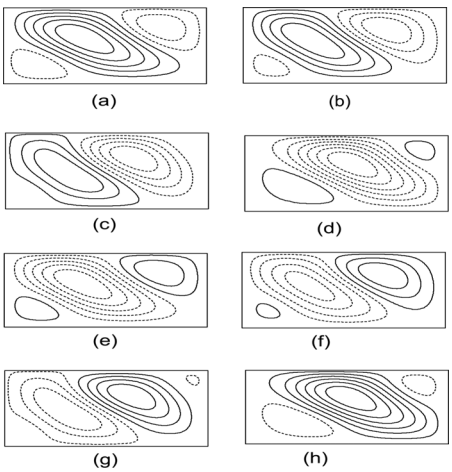

FIG. 4. Flow structure of the eigenfunction at the end of eight successive equal time intervals totaling a full oscillation period when Pr=1, Le=11, and $A=0.5$.

TABLE I. Critical Grashof number (Gr_c) for the onset of convection in a cavity with rigid wall upper boundary (R) and stress-free upper boundary (F). "TR" and "PF" denote the transcritical and pitchfork modes, respectively, while those values in brackets denote the onset of the oscillatory mode.

	Gr_c (R)		Gr_c (F)	
A	TR	PF	TR	PF
0.2	429 084.8	426 778.5	(278 154.7)	
0.3	90 270.9	89 635.8	(59 917.8)	
0.4	31 865.7	30 398.0	(21 288.2)	
0.5	13 922.9	14 405.0	(10 151.0)	
0.6	7 218.0	8 454.9	(5 916.7)	
0.7	4 330.1	5 678.3	3452.6	4440.0
0.8	2 921.5	4 153.9	2382.8	3408.6
0.9	2 160.4	3 215.3	1824.8	2709.4
1.0	1 716.4	2 589.8	1500.3	2222.9
1.2	1 262.5	1 829.7	1165.8	1615.8
1.4	1 058.9	1 407.4	1013.1	1274.2
1.6	957.3	1 152.0	935.6	1069.9
1.8	902.6	999.9	893.6	941.6
2.0	870.2	900.3	(863.4)	
2.2	847.2	835.7	834.0	817.4
2.4	826.4	793.4	814.9	780.6
2.6	804.8	765.9	792.7	757.9
2.8	782.3	748.2	770.5	743.5
3.0	760.8	737.0	750.1	734.5
3.2	741.9	729.9	731.4	729.7
3.4	726.4	724.7	(721.4)	
3.6	714.4	720.3	710.4	717.6
3.8	705.5	715.6	702.6	712.6
4.0	699.1	710.1	697.3	706.7

cillatory flow with very large Gr_c cannot be obtained, the exponentially diverging frequency is also physically impossible.

We also perform a detailed comparison between the onset of convection in a closed cavity and that in the present configuration, as shown in Table I. The results for $1 \le A \le 4$ in the closed cavity have been tabulated by Xin *et al.*[8] (see their Table I), and the present results agree very well with their results. In the range of A studied, there exist three codimension-two points for the closed cavity case: $A=0.47$, $A=2.14$, and $A=3.45$. No new dynamical behavior is observed near these points. When the upper rigid wall is removed, the critical criterion (Gr_c) for both modes decreases, since the upper wall has a stabilizing effect on the equilibrium solution. More importantly, after the removal, near the three original codimension-two points there exist certain ranges of A in which the two steady modes mix into the oscillatory mode (Fig. 3).

For the steady onset of convection, it has been shown by Ghorayeb and Mojtabi[6] that the critical condition is determined by the product $Ra_c(Le-1)$, which depends on A only. However, when the onset of instability is oscillatory, the principle of exchange of stability is no longer valid. The above critical product does not exist and thus the variation of

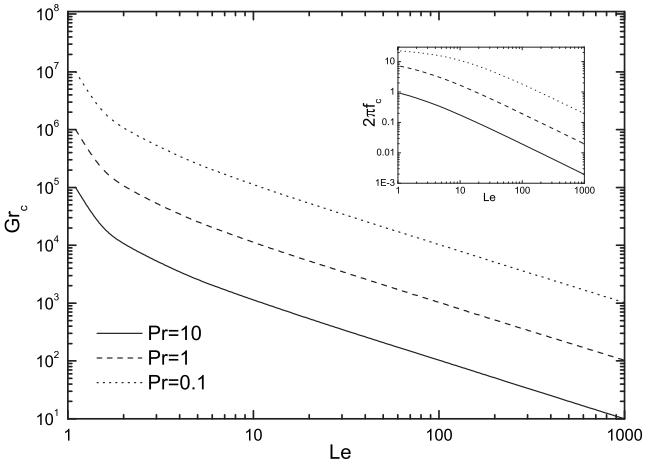

FIG. 5. Neutral stability curves for $A=0.5$ and different Pr values. The variation of the critical frequency is also shown as the inset.

Pr or Le can independently have an effect on the stability of the equilibrium solution. The neutral stability curves showing the influence of Le when $A=0.5$ and Pr=0.1, 1, and 10 are shown in Fig. 5. At this aspect ratio, the onset of instability is oscillatory [Fig. 3(a)]. The critical Gr_c decreases as Le increases, which means that at higher Le the equilibrium is more unstable. This is reasonable and characteristic of double-diffusive instability, since it is the difference of the diffusivity rates of the two components in the fluid that triggers the instability and Le denotes how large this difference is. When the difference vanishes (Le=1), the equilibrium is infinitely stable (very large Gr_c), as is apparent from Fig. 5 when Le decreases toward 1. The flow structure of the eigenfunction along these neutral curves has been verified to be qualitatively the same as that shown in Fig. 4. The variation of the critical frequency is also shown as inset in Fig. 5. Smaller Le value corresponds to larger Gr_c and faster oscillation.

The neutral stability curves showing the influence of Pr when $A=0.5$ and Le=11, 101, and 1001 are shown in Fig. 6. It is interesting that these curves are almost parallel straight lines in this log-log scale. Since the ratio of the diffusivities of heat and solute has been fixed (11, 101, and 1001), smaller Pr value means that heat and solute diffuse faster. Then infinitesimal disturbances of the temperature and concentration field can be dissipated faster, rendering the equilibrium solution more stable. Again, the flow structure of the eigenfunction along these neutral curves has been verified to be qualitatively the same as that shown in Fig. 4, and the critical frequency increases as Pr decreases.

Figures 5 and 6 cover very large ranges of both Le and Pr numbers, and thus the situation for different binary fluids can be expected. For example, for a binary metallic mixture with Pr=0.01 and $Le=10^4$, from Fig. 6 it can be expected that Gr_c is $O(10^3)$, since the three neutral curves for Le=11, 101, and 1001 intersect the left vertical axis at about $Gr_c = 10^6$, 10^5, and 10^4, respectively. Similarly, it can be expected from the inset that $2\pi f_c$ is $O(0.1)$.

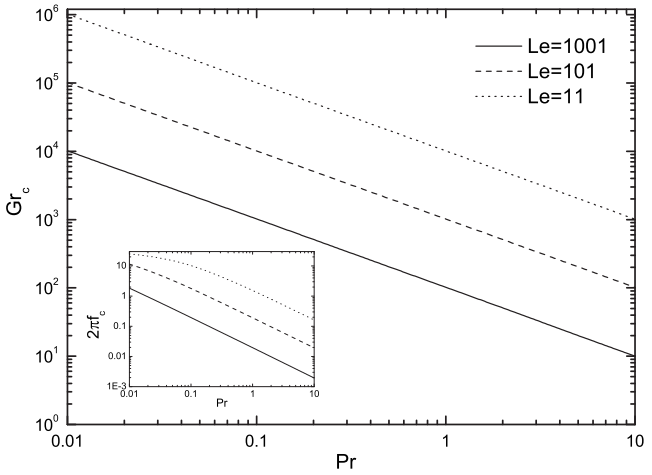

FIG. 6. Neutral stability curves for $A=0.5$ and different Le values. The variation of the critical frequency is also shown as the inset.

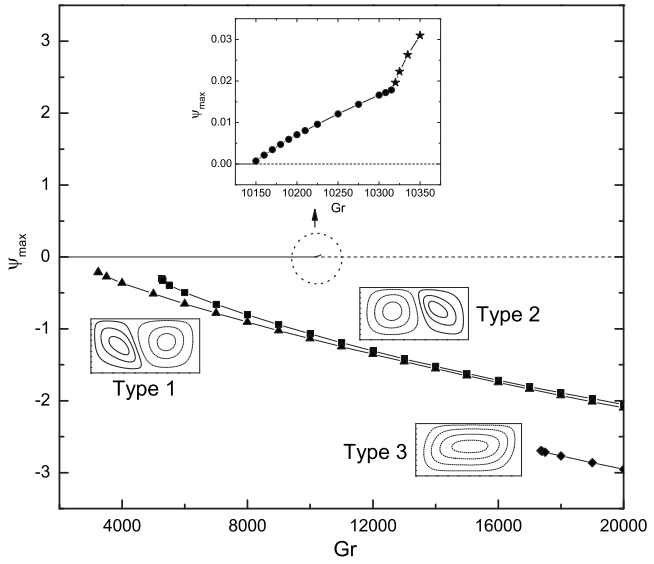

FIG. 8. Maximum stream function vs Gr when Pr=1, Le=11, and $A=0.5$. Solid line denotes stable equilibrium and dashed line denotes unstable equilibrium. The circle points in the inset represent oscillatory flows arising from the supercritical Hopf bifurcation, while the star points represent oscillatory flows after a period-doubling bifurcation. Three different types of steady flows are represented by the triangular, square, and diamond points, respectively, together with the flow structures shown.

B. Direct numerical simulation

1. Oscillatory flow regime

Careful direct numerical simulations have also been performed to verify the linear stability analysis results and to study the nonlinear evolution of the flow field after the onset of convection. It is well known that near a supercritical Hopf bifurcation, the amplitude of the periodic solution is $O(|\mathrm{Gr}-\mathrm{Gr}_c|^{1/2})$,[27] where Gr_c is the critical Grashof number at which a Hopf bifurcation occurs. Using the equilibrium solution as the initial fields, we start direct simulation for Pr=1, Le=11, $A=0.5$, and Gr=10 220. Oscillatory flow is obtained. Then successive runs are performed for decreasing Gr with a step of Δ Gr=10, with the result of the last run as the initial fields of the next run. The square of the saturation amplitude of $u(t,0.5,0.5)$ versus Gr is plotted in Fig. 7. The linear fit intersects the horizontal line at Gr=10 150.0, which agrees extremely well with $\mathrm{Gr}_c=10\,151.0$ (Table I). The critical frequencies by these two different methods are 0.244 and 0.246, respectively. So, indeed, under the present parameter combination the first critical point encountered by the equilibrium solution is a supercritical Hopf bifurcation. The flow structure obtained by direct simulation is exactly the same as that shown in Fig. 4.

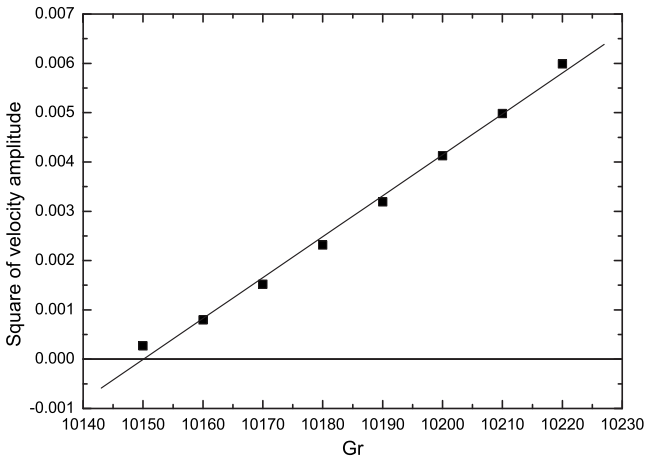

FIG. 7. Square of the amplitude of $u(t,0.5,0.5)$ vs Gr when Pr=1, Le=11, and $A=0.5$. Square points are obtained by direct numerical simulations while the solid line is the linear fit.

With increasing Gr, we continue the simulations from Gr=10 220. The maximum stream function of this oscillatory flow is shown by the circle points in the inset of Fig. 8. When Gr is further increased from 10 310 to 10 320, a period-doubling bifurcation is encountered. This is apparent from Fig. 9 where the time series of $u(0.5,0.5)$ and the corresponding power spectra are shown. When Gr=10 310, the flow is single periodic with a fundamental frequency $f_1=0.230$. When Gr=10 320, f_1 slightly decreases to 0.224 and a subharmonic $f_1/2=0.112$ appears in the power spectrum. The oscillation period doubles after the bifurcation. This new oscillatory flow remains stable up to Gr=10 350 and is represented by the start points in the inset of Fig. 8. When Gr is further increased to 10 360, the oscillatory flow can no longer be preserved and the flow field transits to a steady state. The characteristic of different steady flow states in Fig. 8 will be discussed in Sec. IV B 2.

2. Steady flow regime

Similar to the situation in a vertical closed cavity studied by Ghorayeb and Mojtabi,[6] different subcritical steady states can be obtained in the present configuration. The final convergent steady flow state depends on the initial fields. In order to get as many steady states as possible, we have used random velocity, temperature, and concentration fields to start simulations. The initial value of every physical quantity on a grid point is a random number uniformly distributed in the interval (0, 1). By using such random initial fields, we hope that the solution can be perturbed into the basins of attraction of different steady states. However, we have no

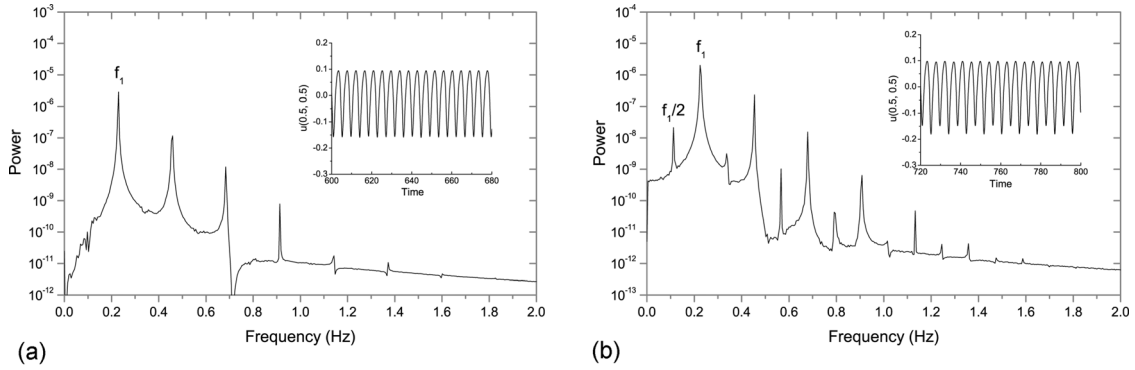

FIG. 9. Time series of $u(0.5,0.5)$ (insets) and the corresponding power spectra when (a) Gr=10 310 and (b) Gr=10 320 for Pr=1, Le=11, and $A=0.5$.

guarantee that such method can reveal all the steady-state solutions of the system. As many as 100 times of repeated runs with random initial fields are carried out for one parameter combination.

Totally three different types of steady solution are found, as shown in Fig. 8. The typical flow fields are also shown as insets. For type 1 steady solution, thermal and solutal buoyancy effects are dominant in the right and left parts of the cavity, generating a clockwise and a counterclockwise rotating vortex, respectively. For type 2 solution, the reverse is true, with a clockwise rotating vortex on the left and a counterclockwise rotating vortex on the right. For type 3 solution, the whole cavity is dominated by thermal buoyancy effect and the flow field consists of a large clockwise rotating vortex. These three steady solutions are induced by finite amplitude disturbances and correspond to much stronger flows when compared to the supercritical oscillatory flows, which are only stable in a small range of Gr. The three steady solution branches start from different Gr values and remain stable at least up to Gr=20 000, which is the maximum parameter investigated.

It should be mentioned that using direct numerical simulation, the bifurcation diagram shown in Fig. 8 is incomplete, since only stable solution branches are presented. While it is clear from linear stability analysis that the oscillatory flow arises from small disturbance via a supercritical Hopf bifurcation, the origins of the different steady solution branches, especially how these branches connect to the equilibrium solution, remain unexplored in the present study. We are currently developing a continuation method to generate a more complete bifurcation diagram, in order to fully explore the different solution branches and to study how the stable solutions lose stability, or how the unstable solutions regain stability.

As Le increases, the onsets of different steady flows are shown in Fig. 10. The neutral curve for Pr=1 in Fig. 5 for the onset of oscillatory flow is also plotted for comparison. It can be seen that these four different curves do not intersect each other and remain well separated. Thus, given appropriate disturbances, small or finite amplitude, type 1 steady, type 2 steady, oscillatory, and type 3 steady flows appear successively as Gr increases. These four curves qualitatively have the same shape.

When A decreases to 0.2, totally four different types of steady solutions are found, as shown in Fig. 11, where the

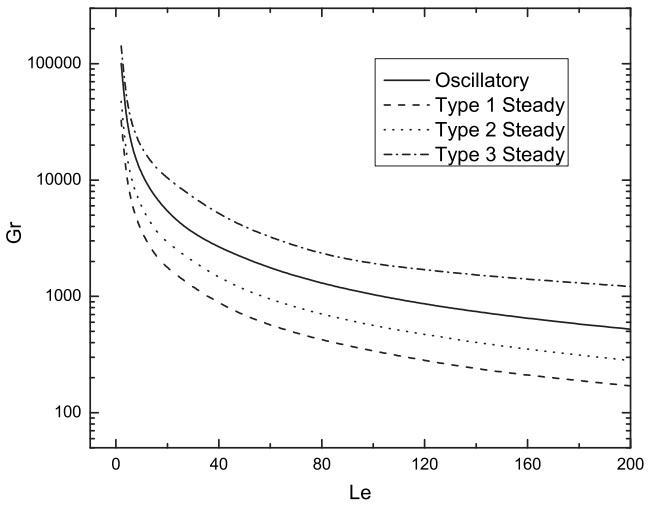

FIG. 10. Onset of different steady and oscillatory flows as Le increases for Pr=1 and $A=0.5$.

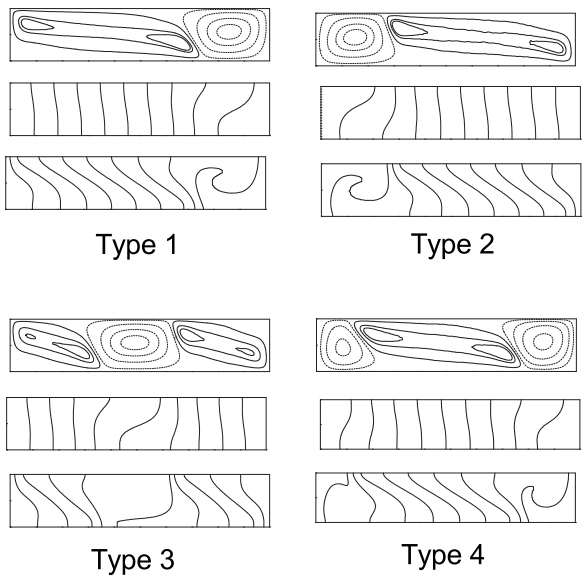

FIG. 11. Contours of stream function (top), temperature (middle), and concentration (bottom) fields showing the multiplicity of steady-state solution for Pr=1, Le=11, $A=0.2$, and Gr=800 000.

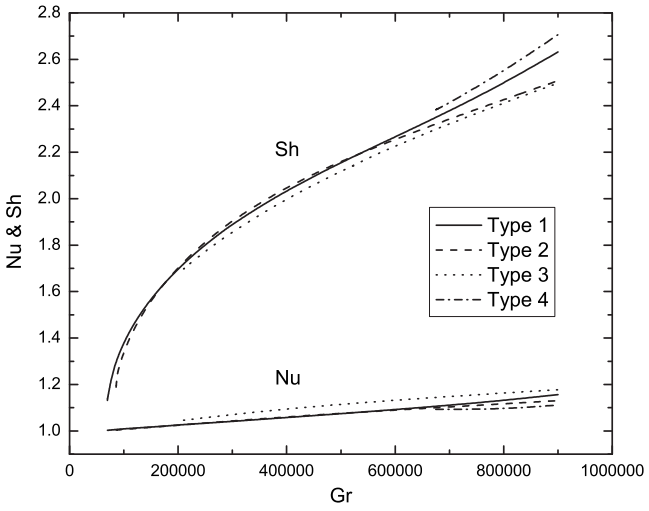

FIG. 12. Variations of Nu and Sh with Gr for four different steady solutions when Pr=1, Le=11, and $A=0.2$.

contours of stream function, temperature, and concentration are plotted for the same parameter set. The most important character of these four different flow structures is that every large counterclockwise rotating vortex consists of two corotating cores. The first two types correspond to the type 1 and type 2 solutions when $A=0.5$, respectively, while the last two types seem to be new. The heat and mass transfer properties of these four steady solutions are shown in Fig. 12 by plotting Nu and Sh versus Gr. Again, given appropriate finite amplitude disturbances, type 1 to type 4 steady flows appear successively as Gr increases. They remain stable at least up to Gr=900 000, and in the range $675\,000 \leq Gr \leq 900\,000$ these four steady states simultaneously exist. The Nu values increase almost linearly while that for the Sh values is clearly nonlinear. The most interesting feature is that while type 3 steady state is most efficient in heat transfer, it is least efficient in mass transfer, and while type 4 steady state is least efficient in heat transfer, it is most efficient in mass transfer. For most part of the parameter range, type 1 and type 2 steady states almost have the same heat transfer rate.

V. CONCLUSIONS

The onset of double-diffusive natural convection in a rectangular cavity with horizontal temperature and concentration gradients is studied in the present work. While the case of a closed cavity has been extensively investigated in existing literatures, that in the present work has a stress-free upper boundary, which is more relevant to many engineering applications. Both linear stability analysis and direct numerical simulation are used and the main results are summarized as follows:

(1) Variations of the leading eigenvalues with Gr are shown. Depending on the cavity aspect ratio, the first two real eigenvalues can merge into a complex coalescence as Gr increases. Then the onset of convection is induced by a supercritical Hopf bifurcation. As Gr further increases, the pair of complex conjugate eigenvalues splits into two real eigenvalues. The two leading steady modes switch place after the splitting. This interesting new phenomenon cannot be observed when the upper boundary of the cavity is a rigid wall.
(2) Neutral stability curves showing the influences of A, Le, and Pr are obtained. There exist some ranges of A in which the first two steady modes mix into an oscillatory mode. Below a critical aspect ratio ($A_c=0.63$), the onset of convection is always oscillatory. The oscillatory flow consists of counter-rotating vortices traveling from right to left and the number of vortices increases as A decreases. The flow structure of the bifurcating eigenfunction does not change qualitatively along the neutral curve when Le or Pr is varied.
(3) The oscillatory flow arising from small amplitude disturbance undergoes a period-doubling bifurcation when Gr is further increased. Only in a small range of Gr does this oscillatory flow regime remain stable.
(4) Many different subcritical steady states are found. They are induced by finite amplitude disturbances and correspond to much stronger flows when compared to the oscillatory regime. The influence of Le on the onset of steady flows and the heat and mass transfer properties are also investigated.

The physical model studied in the present work can be considered a prototype configuration relevant to some horizontal crystal growth techniques, e.g., horizontal Bridgman.[28] An interesting new phenomenon is observed and the results presented can enrich the studies on the onset of double-diffusive convection when the horizontal gradients of temperature and concentration are equal and opposing.[6,8,10]

ACKNOWLEDGMENTS

The work described in this paper was supported by a grant from The Hong Kong Polytechnic University (Project No. G-U666).

[1] J. S. Turner, "Double-diffusive phenomena," Annu. Rev. Fluid Mech. **6**, 37 (1974).
[2] H. E. Huppert and J. S. Turner, "Double-diffusive convection," J. Fluid Mech. **106**, 299 (1981).
[3] J. S. Turner, "Multicomponent convection," Annu. Rev. Fluid Mech. **17**, 11 (1985).
[4] R. Krishnan, "A numerical study of the instability of double diffusive convection in a square enclosure with a horizontal temperature and concentration gradients," *ASME National Heat Transfer Conference*, Philadelphia, 1989 (ASME, New York, 1989), p. 357.
[5] D. Gobin and R. Bennacer, "Double diffusion in a vertical fluid layer: Onset of the convective regime," Phys. Fluids **6**, 59 (1994).
[6] K. Ghorayeb and A. Mojtabi, "Double diffusive convection in a vertical rectangular cavity," Phys. Fluids **9**, 2339 (1997).
[7] K. Ghorayeb, H. Khallouf, and A. Mojtabi, "Onset of oscillatory flows in double-diffusive convection," Int. J. Heat Mass Transfer **42**, 629 (1999).
[8] S. H. Xin, P. Le Quere, and L. S. Tuckerman, "Bifurcation analysis of double-diffusive convection with opposing horizontal thermal and solutal gradients," Phys. Fluids **10**, 850 (1998).
[9] G. Bardan, A. Bergeon, E. Knobloch, and A. Mojtabi, "Nonlinear doubly diffusive convection in vertical enclosures," Physica D **138**, 91 (2000).
[10] A. Bergeon, K. Ghorayeb, and A. Mojtabi, "Double diffusive instability in an inclined cavity," Phys. Fluids **11**, 549 (1999).
[11] M. Mamou, P. Vasseur, and E. Bilgen, "Double-diffusive convection instability in a vertical porous enclosure," J. Fluid Mech. **368**, 263 (1998).
[12] M. Karimi-Fard, M. C. Charrier-Mojtabi, and A. Mojtabi, "Onset of sta-

tionary and oscillatory convection in a tilted porous cavity saturated with a binary fluid: Linear stability analysis," Phys. Fluids **11**, 1346 (1999).
[13]A. Bergeon and E. Knobloch, "Natural doubly diffusive convection in three-dimensional enclosures," Phys. Fluids **14**, 3233 (2002).
[14]A. Bergeon and E. Knobloch, "Spatially localized states in natural doubly diffusive convection," Phys. Fluids **20**, 034102 (2008).
[15]M. Ouriemi, P. Vasseur, A. Bahloul, and L. Robillard, "Natural convection in a horizontal layer of a binary mixture," Int. J. Therm. Sci. **45**, 752 (2006).
[16]T. L. Bergman, "Numerical simulation of double-diffusive Marangoni convection," Phys. Fluids **29**, 2103 (1986).
[17]Z.-W. Chen, Y.-S. Li, and J.-M. Zhan, "Double-diffusive Marangoni convection in a rectangular cavity: Onset of convection," Phys. Fluids **22**, 034106 (2010).
[18]Y.-S. Li, Z.-W. Chen, and J.-M. Zhan, "Double-diffusive Marangoni convection in a rectangular cavity: Transition to chaos," Int. J. Heat Mass Transfer **53**, 5223 (2010).
[19]L. B. Younis, A. A. Mohamad, and A. K. Mojtabi, "Double diffusion natural convection in open lid enclosure filled with binary fluids," Int. J. Therm. Sci. **46**, 112 (2007).
[20]C. Canuto, M. Y. Hussaini, A. Quarteroni, and T. A. Zang, *Spectral Methods in Fluid Dynamics* (Springer, New York, 1988).
[21]J. H. Ferziger and M. Peric, *Computational Methods for Fluid Dynamics* (Springer-Verlag, Berlin, 2002).
[22]L. S. Tuckerman, "Thermosolutal and binary fluid convection as a 2×2 matrix problem," Physica D **156**, 325 (2001).
[23]A. Bergeon, D. Henry, H. Benhadid, and L. S. Tuckerman, "Marangoni convection in binary mixtures with Soret effect," J. Fluid Mech. **375**, 143 (1998).
[24]R. E. Ecke, F. Zhong, and E. Knobloch, "Hopf bifurcation with broken reflection symmetry in rotating Rayleigh-Benard convection," Europhys. Lett. **19**, 177 (1992).
[25]H. F. Goldstein, E. Knobloch, I. Mercader, and M. Net, "Convection in a rotating cylinder. Part 1. Linear theory for moderate Prandtl numbers," J. Fluid Mech. **248**, 583 (1993).
[26]H. F. Goldstein, E. Knobloch, I. Mercader, and M. Net, "Convection in a rotating cylinder. Part 2. Linear theory for low Prandtl numbers," J. Fluid Mech. **262**, 293 (1994).
[27]J. Guckenheimer and P. Holmes, *Nonlinear Oscillations, Dynamical Systems, and Bifurcations of Vector Fields* (Springer, New York, 1983).
[28]Y. Kamotani, L. W. Wang, S. Ostrach, and H. D. Jiang, "Experimental study of natural convection in shallow enclosures with horizontal temperature and concentration gradients," Int. J. Heat Mass Transfer **28**, 165 (1985).